Chinese Chemical Letters 37 (2026) 112196

Contents lists available at ScienceDirect

Chinese Chemical Letters

journal homepage: www.elsevier.com/locate/cclet

Hydrated salt hydrogel with switchable stiffness and tunable thermal performance for environmental low-grade thermal management

Yifan Liu[a,1], Jiazuo Zhou[a,1], Ziyao Wang[a], Lei Qiao[a], Yudong Li[a], Yuan Yu[a], Cong Li[a], Jinliang Zhu[a], Yuehe Gu[a], Xiaohan Sun[b], Haiyue Yang[a,*], Chengyu Wang[a,*]

[a] Key Laboratory of Bio-based Material Science and Technology of Ministry of Education, Northeast Forestry University, Harbin 150040, China
[b] School of Chemical Engineering, University of Chinese Academy of Sciences, Beijing 100049, China

ARTICLE INFO

Article history:
Received 4 July 2025
Revised 13 October 2025
Accepted 27 November 2025
Available online 2 December 2025

Keywords:
Hydrated salt gel
Phase change materials
Mechanical properties
Low-grade heat
Thermal management

ABSTRACT

To reduce the pollution of waste heat to the environment and achieve Sustainable Development Goals, recovering and utilizing of low-grade heat is critical. Although various thermal conversion technologies have been extensively developed, research on thermal energy storage materials with dynamically adjustable properties for diverse applications is still lacking. Herein, hydrated salt hydrogel with switchable stiffness and tunable thermal performance was fabricated by simply incorporating sodium acetate trihydrate into hydrogel network. Hydrated salt hydrogel displayed adjustable thermal performance (maximum heat release temperature from 53 °C to 20 °C; enthalpy value from 0 to 179 J/g) by regulated sodium acetate trihydrate concentration of hydrogels. Moreover, the control of variable mechanical strength (0.03–5.21 MPa) and toughness (0.02–420.58 MPa) was accomplished. The study further demonstrates the promising application of hydrated salt hydrogel in thermal management for electronics and controllable soft-rigid coupling thermoelectric devices, opening new opportunities in waste heat recovery and achieving Sustainable Development Goals.

© 2026 Published by Elsevier B.V. on behalf of Chinese Chemical Society and Institute of Materia Medica, Chinese Academy of Medical Sciences.

Heat is a ubiquitous phenomenon in our daily life, such as in on-body and constructive thermal environments [1–4]. However, about 63 % of heat that is regarded as the low-grade heat gets overlooked as waste heat, and dissipates into the surrounding environment [5–7], resulting in huge energy wastage and violating to Sustainable Development Goals (SDGs) [8] (Fig. 1a). Hence, various thermal energy storage materials have been widely studied for recovering waste heat, reducing environment pollution [9–11], improving the energy efficiency and reducing energy consumption. Thermal energy storage materials mainly undertake the task of collection, storage, transportation and utilization of heat energy. Scientists often integrate phase change materials (PCMs) [12,13] and functional materials to complete thermal management of aeronautics [14], batteries [15], buildings [16], human bodies [17], *etc.* However, thermal energy storage materials lack adjustable stiffness and tunable thermal performance, which are crucial parameters for diverse dynamic application.

Hydrogels have attracted increasing attention due to their smart, variable stiffness and wide range of applications in different fields [18–20], which can be achieved by introducing functional or responsive polymers [21], intelligent fillers [22,23], *etc.* Among them, hybridize hydrogel using crystals is considered to be an effective modification strategy [24]. The growth and disappearance of crystals endow hydrogels with many fascinating functions [25–29] such as thermal control, switchable conductivity, transparency, adhesion, wide range of adjustable mechanical properties. Especially, crystalline hybrid hydrogels would emerge more amazing feature, when the crystal morphologies, contents, and rate of growth are controllable. For example, Cui's group [30] fabricated a time-dependent crystal hydrogels that can automatically change their mechanical properties by controlling the evolution of fibrous crystals into isolated bulk crystals. Ko *et al.* [31] prepared a gradient stiffness-programmed and stretchable electronics integration circuit board by spatially controlling the crystallization-melting of supercooled hydrogel. Therefore, adjustable stiffness and tunable thermal performance should occur within the crystal hydrogels under controlled content of crystals.

Herein, we report a cellulose-hydrous salt gel (cel-sal gel) with mechanical switchable, tunable thermal performance, long-term storage and self-healing, in which sodium acetate trihydrate

* Corresponding authors.
E-mail addresses: haiyueyang@nefu.edu.cn (H. Yang), wangcy@nefu.edu.cn (C. Wang).
[1] These authors contributed equally to this work.

https://doi.org/10.1016/j.cclet.2025.112196
1001-8417/© 2026 Published by Elsevier B.V. on behalf of Chinese Chemical Society and Institute of Materia Medica, Chinese Academy of Medical Sciences.

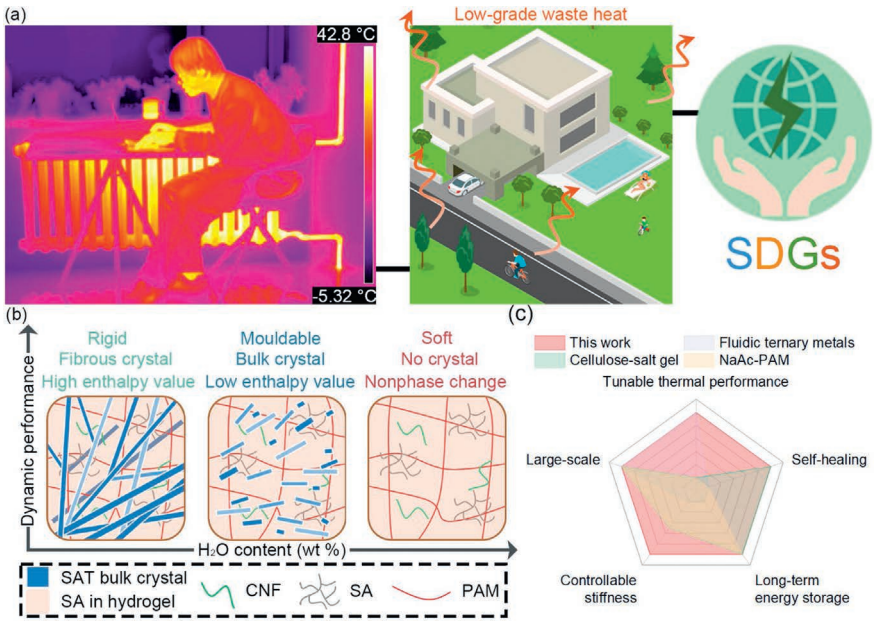


Fig. 1. Design of hydrogels with adjustable stiffness and thermal properties for low-grade thermal management. (a) Schematic of the typical environment of human life. Infrared images showing the production of a large amount of low-grade waste heat due to anthropogenic activities. Collection of this low-grade waste heat contributes to the reduction of carbon emissions to achieve SDGs. (b) Schematic of the material properties within hydrogels, accompanied with the changes in water content. (c) Illustration of the prominent advantage of cel-sal gel compared to other PCMs [32–34].

(SAT) is used as a PCM (molten state-crystalline state) in cellulose nanofibers (CNFs)/starch (SA)/acrylamide (AM) hydrogel. Furthermore, starch gelatinization produces a large number of hydrogen bonds that endow the gel with good self-healing properties, which greatly extends its service-life. CNFs promote the formation of a large number of hydrogen bonds, which contribute to the stability of the shape of hydrogel in the melting state. The morphology, and the rate of growth of SAT crystals could be regulated by concentration. By simply adjusting the content of water, the cel-sal $gel_{x:y}$ (x:y refers to the mass ratio of SAT to water) shows a unique adjustable thermal performance including tunable exothermic temperature, latent heat and melting temperature (Fig. 1b). Interestingly, the phase diagram provides a convenient way to theoretically predict and tune the melting range and the latent heat of cel-sal gel. Additionally, the SAT crystals mainly act as functional fillers and prefer to stiffen the hydrogels due to their rigid nature. When the concentration of sodium acetate changes, the tensile strength can be regulated from soft to rigid. Furthermore, the cel-salt gel is convenient for large-scale preparation (Fig. S1 in Supporting information). This cel-sal gel addresses limitations regarding tunable thermal performance, controllable stiffness, long-term energy storage, self-healing and large-scale (Fig. 1c and Table S1 in Supporting information) posed by traditional thermal energy storage materials and pave the way for diverse applications in efficient low-grade thermal management and contribute to achieve SDGs [32–34].

A series of hydrogels with different SAT and water were prepared using thermal initiation (Fig. S2 in Supporting information). The products were denoted as cel-sal $gel_{x:y}$ (x:y refers to the mass ratio of SAT to water). For example, cel-sal $gel_{9:1}$ was the sample prepared from a precursor containing 73.77 wt% SAT and 8.20 wt% water (*e.g.*, 13.5 g SAT, 1.5 g water, 3.0 g AM, 0.15 g SA, and 0.15 g CNF suspension). When the cel-sal gel cooled down naturally under ambient conditions, it was difficult for SAT to spontaneously form crystal nucleus due to the high nucleation energy barrier, and thus supercooled SAT ensured long-term energy storage. Upon stimulus (contacting with SAT crystal seeds or foreign objects), the barrier could be overcome and the cel-sal gel underwent fast crystallization, changing the hydrogels from transparent and soft to opaque and rigid (Fig. S3 in Supporting information). And the crystallized hydrogels with opaque and rigid state could revert to the transparent and soft state at melting temperature. As the SAT:water ratio changed from 10:0 to 5:5, the cel-sal gel exhibited different states, micro-morphologies (Fig. 2a) and exothermic temperatures (Fig. 2b). To fully understand the effect of concentration on SAT/water mixture and the phase transition behavior of cel-sal gel, the step cooling experiments and theoretical analysis of phase diagrams [35,36] for SAT and water are shown in Fig. 2 and Fig. S4 (Supporting information). Fig. S4 depicts the variation of temperature during the triggering of the crystallization process of the supercooled SAT/water mixture with different water contents. The maximum discharging temperature reached the value of 58 °C for the SAT:H_2O = 10:0 sample, followed by 55, 51, 39, and 28 °C for SAT:H_2O = 9:1, SAT:H_2O = 8:2, SAT:H_2O = 7:3 and SAT:H_2O = 6:4 samples, respectively. Meanwhile, when SAT:H_2O = 5:5, the phase change performance will be lost due to the presence of too much water. Figs. S5 and S6 (Supporting information) show the photos and optical microscope images of SAT/water mixture with different water contents in crystalline states. When SAT:H_2O = 10:0, the crystalline SAT/water mixture was white and the crystals were compact and ordered. As the water content increased, the crystalline SAT/water mixture gradually changed from opaque to transparent and the morphology of crystals changed from dense and fibrous crystals to loose, and isolated bulk crystals. When SAT:H_2O = 6:4, the phase separation process occurred and the white SAT crystals settled to the bottom of the bottle. When SAT:H_2O = 5:5, the SAT/water mixture lost its ability to crystallize with transparent state. These results indicate that the ability of SAT to crystallize gradually decreases with the increase of water content. Therefore, it is completely feasible to adjust the thermal performance of SAT by simply controlling the content of water.

Interestingly, the binary phase diagram provides a convenient way to explain and predict the melting temperature and latent heat of sodium acetate/water mixture, making effective utilization of the latent heat in different thermal environments. As shown in Fig. 2c, SAT had the salt mass fraction of 0.603 and the congruent

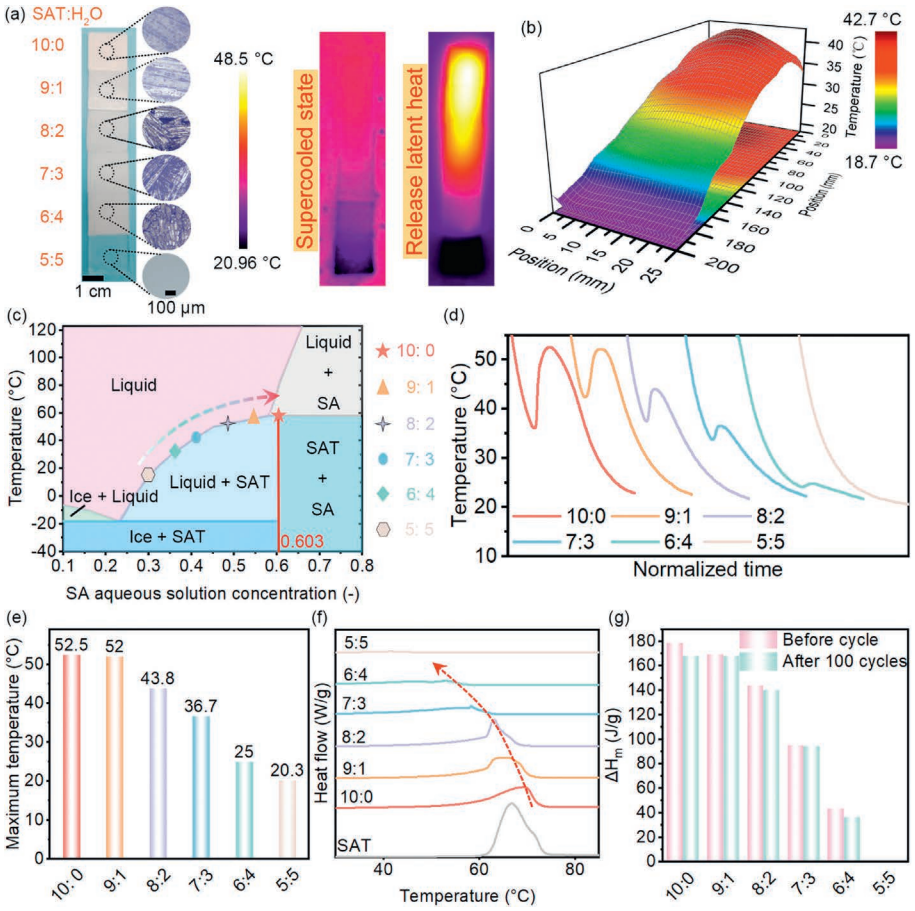


Fig. 2. Cel-sal gel with adjustable thermal properties. (a) Photos, optical microscope images and infrared images of cel-sal gel. Cel-sal gel with different water contents are combined by self-healing. (b) Maximum exothermic temperature of cel-sal gels with different water contents. (c) Phase diagram of sodium acetate aqueous solution. (d) Step-cooling curves of cel-sal gel. (e) Temperature profiles showing the cel-sal gel with different water contents have different maximum discharge temperatures. (f) DSC heating curves for cel-sal gels with different water content. (g) Enthalpy values for cel-sal gels with different water content before and after 100 heating-cooling cycles.

melting point of 58.0 °C. The phase diagram was divided into six areas, including liquid sodium acetate aqueous solution area, liquid sodium acetate aqueous solution and solid sodium acetate area, liquid sodium acetate aqueous solution and solid SAT area, solid SAT and solid sodium acetate area, liquid sodium acetate aqueous solution and solid ice area, solid SAT and solid ice area. For SAT with extra water (sodium acetate aqueous solution with concentration lower than 0.603 by weight), with the decrease in the concentration of the solution, the phase equilibrium temperature reduced, and the lowest equilibrium temperature was the eutectic melting point of ice-SAT binary system, which was −18.0 °C at the sodium acetate concentration of 0.233 by weight. In general, since the thermal properties of SAT are affected by the concentration of sodium acetate, the PCMs with specific thermal properties can be prepared by the guidance of phase diagram.

However, the SAT/water mixture tends to leak in the melted state, which is inconvenient in practical applications. The SAT/water mixture was combined with PAM crosslinked network, SA and CNF to prepare cel-sal gel. Fig. 2d shows the step cooling curve of cel-sal gel, which reveals a similar trend as the cooling curve of the SAT/water mixture. The maximum discharging temperature reached 52.5 °C for the cel-sal $gel_{10:0}$, followed by 52.0, 43.8, 36.7, and 25.0 °C for the cel-sal $gel_{9:1}$, cel-sal $gel_{8:2}$, cel-sal $gel_{7:3}$ and cel-sal $gel_{6:4}$, respectively (Fig. 2e). In addition, the PAM network will restrict the SAT crystallization. The heat release temperature of the cel-sal gel was generally lower than the SAT/water mixture. Infrared thermal imager was used to record the crystalline behavior of the cel-sal gel (5 cm × 2 cm × 3 mm; Fig. S7 in Supporting information). The rate of crystallization can be affected by the content of water. It takes 250 s for cel-sal $gel_{10:0}$ to crystallize, while cel-sal $gel_{9:1}$ takes 125 s to crystallize. However, crystallization time of cel-sal $gel_{8:2}$ (75 s), cel-sal $gel_{7:3}$ (125 s) and cel-sal $gel_{6:4}$ (400 s) increased with the increase of water content. As a result, the rate of growth of the crystal was measured, as shown in Fig. S8 (Supporting information). Cel-sal $gel_{10:0}$ and cel-sal $gel_{9:1}$ had similar rates of growth of crystal. For cel-sal $gel_{8:2}$, cel-sal $gel_{7:3}$ and cel-sal $gel_{6:4}$, the rate of growth of crystal decreased with the increase in water content. Generally, reasons followed: First, the maximum discharging temperature of cel-sal $gel_{10:0}$ and cel-sal $gel_{9:1}$ reached the values of 52.5 and 52.0 °C, which were close to the melting temperature (58 °C). Consequently, the crystallizations of cel-sal $gel_{10:0}$ and cel-sal $gel_{9:1}$ were hindered, and the rate of crystallization became very slow. However, the maximum discharging temperature of cel-sal $gel_{8:2}$ rarely reach the value of 43.8 °C, which was lower than the melting temperature and it will no longer restrict the crystallization process. Hence, the rate of growth of cel-sal $gel_{8:2}$ suddenly increased. Second, for cel-sal $gel_{8:2}$, cel-sal $gel_{7:3}$ and cel-sal $gel_{6:4}$, the higher water content meant lower concentrations of sodium acetate, the longer time it takes the solute molecules to reach the crystal surface, and the slower the rate of crystallization. As shown in Fig. 2f and Table S2 (Supporting information), differential calorimetric scanner (DSC) curves showed that the melting temperature of cel-sal gel decreased gradually with the increase of water content. The in-

crease of water content led to the melting process of sodium acetate accompanied by dissolution, and more water made sodium acetate to dissociate more easily into ions, so the melting temperature was lower. After 100 heating and cooling cycles, cel-sal gel showed nearly the same patterns and melting behaviors, indicating its excellent thermal stability (Fig. 2g, Fig. S4b and Table S2 in Supporting information). The enthalpy value was proportional to the concentration of sodium acetate (Fig. 2g). Furthermore, the self-healing properties (Figs. S9 and S10 in Supporting information) of the gel can integrate cel-sal gel with different water content, so that it is more designed and collaborative (Fig. S11 and Note 1 in Supporting information). These results showed that the cel-sal gel as thermal energy storage materials has controllable thermal performance for diverse dynamic applications.

Furthermore, the transmittance of the crystallized hydrogel within the visible wavelength range improved dramatically with the increase in water content (Figs. S12 and S13 in Supporting information). The increased transparency of the gel stood for the decreased crystal content. The content of the free water of crystallized cel-sal gel was measured by low-field nuclear magnetic resonance (LF-NMR) according to the differences in the relaxation time between free water and bound water (including crystal water) (Fig. S14 in Supporting information). When the water content was low, the water molecules were almost completely bound to the SAT lattice. As the water content increased, the content of free water and the electrical conductivity increased (Fig. S15 in Supporting information), indicating that the increase of water content caused more sodium acetate to dissolve in the water and be dissociate into ions. As a result, when SAT:H_2O = 5:5, all sodium acetate was dissolved in water and lost its ability to crystallize. The surface morphology of the cel-sal gel was observed using scanning electron microscope (SEM; Fig. S16 in Supporting information) and optical microscope (Fig. S17 in Supporting information). As the water content increased, the crystals gradually changed from fibrous compact, ordered, and regular to bulk, loose, small, and more irregular in shape. As shown in Fig. S18 (Supporting information), the relative peak intensities of XRD patterns declined with the increase water content, indicating that the crystallinity of SAT crystals decreased with the addition of water, further confirming the inhibitory effect of water on crystallization. In summary, water critically influences the crystal structure of sodium acetate trihydrate. By affecting sodium acetate solubility, it governs crystal morphology, crystallization rate, and the maximum exothermic temperature. Consequently, controlling water content allows effective regulation of the gel's thermal properties.

Considering that the distribution of the operating temperature of daily electronic products varies within the range of 20–90 °C, it is important to select the thermal energy storage materials with corresponding phase transition temperature and enthalpy values. When the phase change temperature was higher than the operating temperature of the electronic product, there was no phase change and no latent heat storage. When the phase change temperature was much lower than the operating temperature of the electronic product, a large amount of sensible heat was dissipated. The controllable thermal performance of cel-sal gel made it suitable for collecting low-grade heat in household applications (Fig. 3), while the cel-sal gel could be customized according to the operating temperature of the electronic product. For example, cel-sal $gel_{10:0}$ (melting temperature of 69.25 °C and enthalpy value of 178.59 J/g) was suitable for collecting waste heat generated by the CPU at an operating temperature of 70–90 °C, rather than the waste heat generated by the USB flash disk at an operating temperature of about 40 °C. Since the waste heat generated by the CPU was enough to melt the PCMs in the cel-sal $gel_{10:0}$, the cel-sal $gel_{10:0}$ would store the waste heat to transit to supercooled state for long time. However, the temperature of waste heat generated by the USB flash disk was too low to cause the phase transition. Therefore, the sensible heat was immediately lost to the environment rather than stored by PCMs. As shown in Figs. 3a-e, when the CPU was operating, cel-sal $gel_{10:0}$ ($45 \times 37.5 \times 2\ mm^3$) was used to prevent thermal runaway. The infrared photos and real-time temperature curves of the CPU running for 5.5 min are shown in Figs. 3a, b and e. The running CPU without cel-sal $gel_{10:0}$ showed the highest temperature (around 100 °C) within 50 s (Figs. 3a, b and e). In contrast, the temperature of the CPU with cel-sal $gel_{10:0}$ increased from approximately 20 °C to 50 °C in the initial 120 s, after which, it stabilized at nearly 51 °C in 3 min. The results showed that the CPU with cel-sal $gel_{10:0}$ had low rate of increase in temperature and peak temperature, which was due to the phase change of cel-sal $gel_{10:0}$ absorbing and storing waste heat (Figs. 3c, d and e). The cel-sal $gel_{10:0}$ provided effective low-grade thermal management during the operation of the CPU. However, the cel-sal $gel_{6:4}$ showed weak thermal management for CPU with peak temperature of 91.99 °C, which was due to the low enthalpy (43.63 J/g) and low melting temperature (44.86 °C) of the cel-sal $gel_{6:4}$ (Fig. 3e). Therefore, selecting appropriate cel-sal gels is crucial for thermal management of electronics at different operating temperatures.

As shown in Figs. 3f-j, the cel-sal $gel_{6:4}$ ($37 \times 12 \times 2\ mm^3$) was applied for thermal management of USB flash drive to prevent overheating. The temperature of the USB flash disk without cel-sal $gel_{6:4}$ reached the value of 41 °C after 700 s. The USB flash disk with cel-sal $gel_{6:4}$ showed slower rate of increase in temperature. The maximum temperature difference at 550 s between the USB flash disk with and without the cel-sal $gel_{6:4}$ could be approximately 3 °C (40 °C *vs.* 37 °C). The melting temperature of the cel-sal $gel_{6:4}$ was 44.86 °C, which corresponded to the operating temperature of the USB flash disk. Therefore, the waste heat generated during the operation of USB flash disk could cause the phase transitioning of cel-sal $gel_{6:4}$, which absorbed a lot of heat energy and reduced the operating temperature of USB flash disk. However, when the cel-sal $gel_{10:0}$ was used for the thermal management of USB flash disk, the temperature of the USB flash disk reached approximately 40.3 °C after 700 s with similar rate of increase in temperature, which was only 0.7 °C lower than the case when USB flash disk did not have any cel-sal gel. The running temperature of USB flash disk was lower than the melting temperature of cel-sal $gel_{10:0}$ with no phase change, thus the cel-sal $gel_{10:0}$ could not perform effective thermal management for the USB flash disk. Therefore, choosing the appropriate cel-sal gel is crucial, which can not only effectively collect and store waste heat, but also reduce the working temperature of electronic products to extend their life-service lives. These results show that the cel-sal gels with different water contents can effectively relieve the overheating of electronic, which has great potential applications in low-grade thermal management.

The morphology and content of crystals play an essential role in determining the mechanical properties of hydrogel. Hydrogels are typically soft and elastic. The introduction of crystals with different contents and morphologies was expected to stiffen and toughen the hydrogels to different degrees. As shown in Fig. 4a and Figs. S19 and S20 (Supporting information), the tensile strength and Young's modulus of cel-sal $gel_{10:0}$ had values of 5.21 and 420.58 MPa, respectively, while the corresponding value for cel-sal $gel_{5:5}$ were 0.03 and 0.02 MPa, respectively. The crystal reinforced cel-sal $gel_{10:0}$ showed 174-times higher tensile strength and 21,029-times higher stiffness than the soft cel-sal $gel_{5:5}$. As the water content increased, the tensile strength and Young's modulus decreased. As shown in Fig. 4b and Fig. S21 (Supporting information), compressive strength showed a similar variation trend. The rigid crystals formed within polymer networks could stiffen matrices, while excess water will dissolve crystals and soften the gel. In

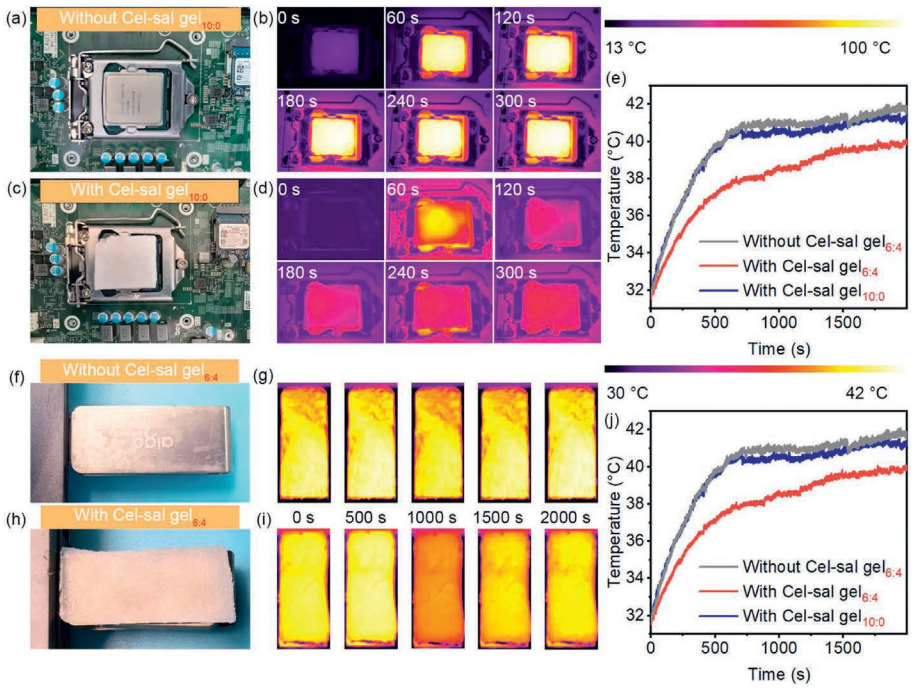


Fig. 3. Cel-sal gels for the thermal management of electronics. (a) Photograph of the motherboard from a desktop computer. The center unit is a CPU. (b) Infrared images of the CPU without cel-sal $gel_{10:0}$ when the CPU ran at 100% usage. (c) Photograph of the CPU with cel-sal $gel_{10:0}$. (d) Infrared images of the CPU with cel-sal $gel_{10:0}$ when the CPU ran at 100% usage. (e) The real-time temperature of the CPU was monitored. (f) Photograph of the USB flash disk. (g) Infrared images of the USB flash disk without cel-sal $gel_{6:4}$. (h) Photograph of the USB flash disk with cel-sal $gel_{6:4}$. (i) Infrared images of the USB flash disk with (i) cel-sal $gel_{6:4}$. (j) Real-time temperature of the USB flash disk was monitored.

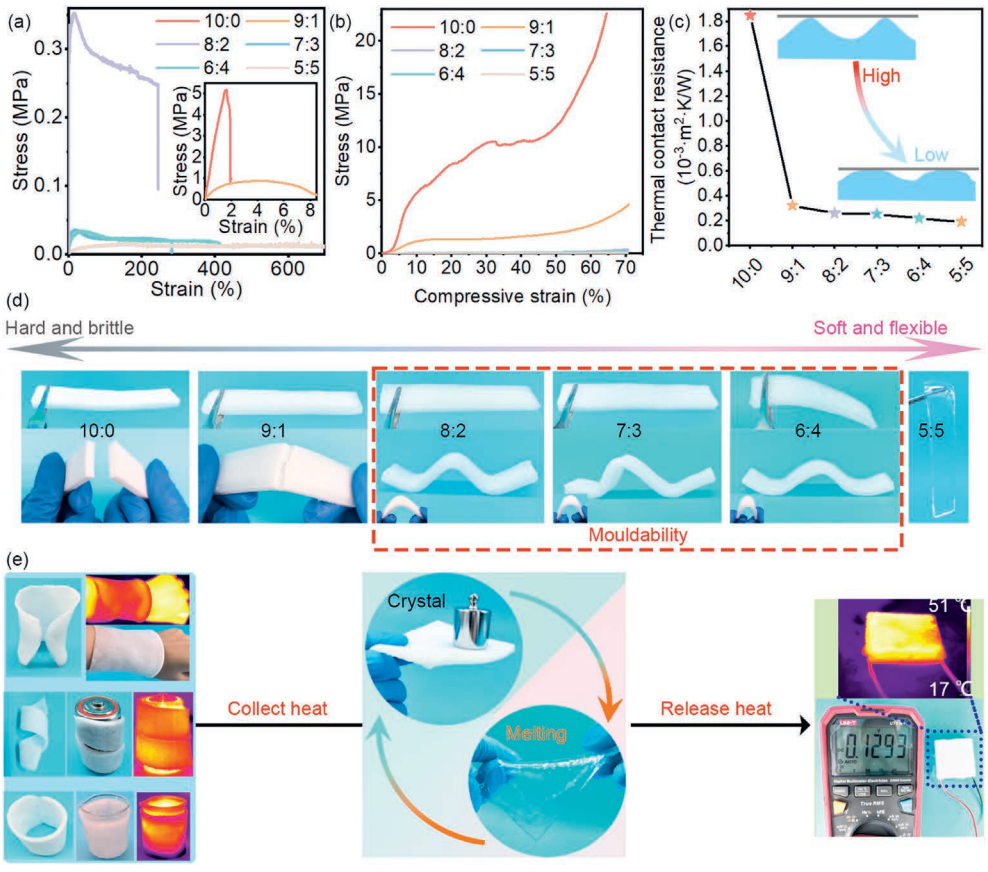


Fig. 4. Cel-sal gel with adjustable mechanical properties. (a) Tensile curve of cel-sal $gel_{10:0}$, cel-sal $gel_{9:1}$, cel-sal $gel_{8:2}$, cel-sal $gel_{7:3}$, cel-sal $gel_{6:4}$ and cel-sal $gel_{5:5}$. (b) Compression curves of cel-sal $gel_{10:0}$, cel-sal $gel_{9:1}$, cel-sal $gel_{8:2}$, cel-sal $gel_{7:3}$, cel-sal $gel_{6:4}$ and cel-sal $gel_{5:5}$. (c) Thermal contact resistance of the cel-sal gel. (d) Graphs of the cel-sal gel for shape fixation. (e) Cel-sal gel for complex temporary shape fixation to collect low-grade waste heat and for thermoelectric power generation through crystallization-melting transition.

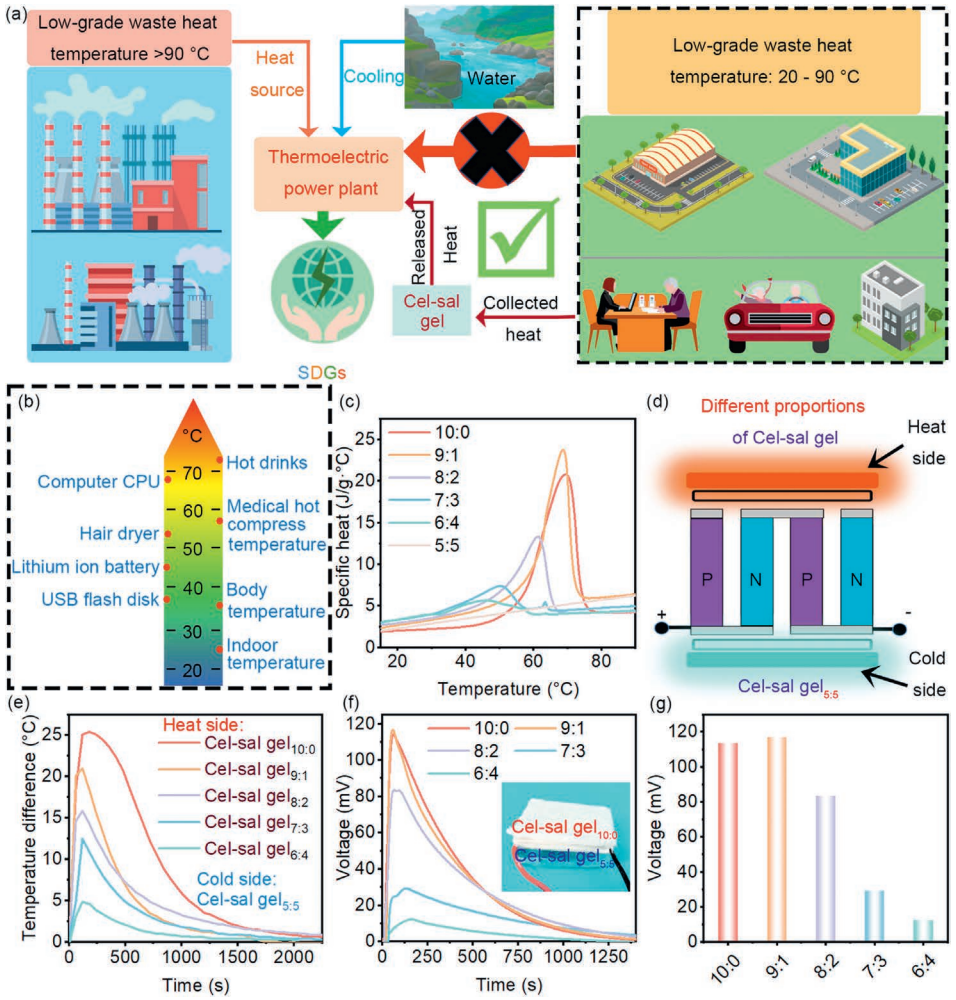


Fig. 5. Cel-sal gel for thermal power generation. (a) Schematic shows that low-grade heat with a temperature higher than 90 °C is used for thermoelectric power generation. However, low-grade heat at temperatures <90 °C is often not used for thermal power generation. Cel-sal gel can be used to collect low-grade heat at temperatures below 90 °C, and then, be used for thermal power generation. (b) Service-temperatures of various objects. (c) The specific heat of cel-sal gel. (d) Schematic of the mechanism shows the cel-sal gel is used for thermoelectric power generation. (e) Temperature difference-time curves of cel-sal gel in thermoelectric power generation. (f) Output voltage curves of the cel-sal gel. (g) Output voltage of the cel-sal gel.

conclusion, crystals utilized as fillers exert a significant influence on the mechanical properties of gels. Consequently, the mechanical properties can be effectively regulated by modifying the crystal morphology through controlled water content.

Fig. 4c shows the dynamic changes in the thermal contact resistance of the cel-sal gel, which is enabled by the changes in dynamic modulus of the cel-sal gel with the increase in water content. The low contact surface between cel-sal $gel_{10:0}$ and electronics caused high thermal contact resistance (1.85×10^{-3} m^2 K W^{-1}), which was due to the high modulus of the cel-sal $gel_{10:0}$ in the rigid state. As the water content increased, the gel switched to the soft state, resulting in an increase in the contact area with lower thermal contact resistance. In addition, cel-sal $gel_{8:2}$, cel-sal $gel_{7:3}$ and cel-sal $gel_{6:4}$ showed excellent formabilities (Fig. 4d). Moreover, cel-sal $gel_{10:0}$ and cel-sal $gel_{9:1}$ were rigid and inflexible to fracture under large deformations, while cel-sal $gel_{5:5}$ was too soft and flexible with too much water. By integrating different cel-sal gels, it has demonstrated great development prospects in the field of flexible electronics (Note 2 in Supporting information). For cel-sal $gel_{8:2}$, cel-sal $gel_{7:3}$ and cel-sal $gel_{6:4}$, these crystalline cel-sal gel with moldability and low contact thermal resistance could withstand deformation, and collected waste heat efficiently. For example, the cel-sal $gel_{8:2}$ was adapted to the surface of hand joints, batteries, and beakers (Fig. 4e). The moldable cel-sal gel could be fitted onto curved surfaces to collect low-grade waste heat and generate electric energy by crystallization-melting transition.

Low-temperature heat recovery, including the recovery and utilization of low-grade heat energy (200 °C), achieves energy-saving and reduction in its consumption in industrial processes [1,37]. Low-grade heat above 90 °C is easily converted into heat energy due to its high heat density and concentration (Fig. 5a). However, about 63 % of low-grade heat of 20–90 °C (Fig. 5b) is often wasted due to dispersion and low heat density [7,38]. Therefore, it is necessary to utilize low-grade heat of 20–90 °C with thermal energy storage materials that can address the mismatch between heat supply and demand in aspects of time, space, and intensity. In this work, cel-sal gel with switchable stiffness and tunable thermal performance were found suitable for collecting low-grade waste heat range from 20 °C to 90 °C. As shown in Fig. 5c, the curves of cel-sal $gel_{10:0}$ and cel-sal $gel_{9:1}$ showed an obvious specific thermal jump signal near 70 °C, which corresponded to the phase transition of SAT. The specific heat jump signals of cel-sal $gel_{8:2}$, cel-sal $gel_{7:3}$ and cel-sal $gel_{6:4}$ appeared at about 60, 50, and 40 °C, respectively. The jump signal of the cel-sal gel indicated that different cel-sal gel were suitable for collecting waste heat at corresponding temperature levels. The collection of low-grade waste heat corresponding to the temperature level not only absorbs more heat when the

unit temperature is raised, but also provides more heat when it is used as the heating side for the thermoelectric plate. The specific heat of the cel-sal $gel_{5:5}$ was relatively stable, and there was no specific heat jump signal. In addition, its specific heat (2.107 J g^{-1} °C^{-1}) was larger than that of air (1.006 J g^{-1} °C^{-1}), which was suitable for the cold side of thermoelectric plate. The supercooled cel-sal $gel_{10:0}$, cel-sal $gel_{9:1}$, cel-sal $gel_{8:2}$, cel-sal $gel_{7:3}$ and cel-sal $gel_{6:4}$ (as hot side), and cel-sal $gel_{5:5}$ (as cold side) were integrated for thermoelectric power generation (Fig. 5d). As shown in Fig. 5e and Fig. S22 (Supporting information), the heat release temperature of cel-sal gels with different water contents resulted in different temperature differences(cel-sal $gel_{10:0}$:25.00 °C, cel-sal $gel_{9:1}$:20.79 °C, cel-sal $gel_{8:2}$:15.66 °C, cel-sal $gel_{7:3}$:12.24 °C, and cel-sal $gel_{6:4}$:4.84 °C) between the hot and the cold sides. In addition, the generating voltages of cel-sal $gel_{10:0}$, cel-sal $gel_{9:1}$, cel-sal $gel_{8:2}$, cel-sal $gel_{7:3}$ and cel-sal $gel_{6:4}$ were 113, 117, 83, 30, and 13 mV, respectively (Figs. 5f and g). The results showed that the cel-sal gel was not only suitable for collecting low-grade heat but also provided adjustable voltage supply, which has great application potential in different scenarios and shows great prospects for collecting and utilizing the ignored low-grade heat in our daily-lives to reduce carbon emissions.

In this work, cel-sal gel with switchable stiffness and controllable thermal performance was synthesized to collect and utilize low-grade heat. The water content played a vital role in the regulation of thermal properties and crystal morphology, which also dynamically tuned the mechanical properties of the hydrogel. The phase diagram provided a convenient way to theoretically predict and tune the thermal performance of the hydrogel including tunable exothermic temperature, latent heat and melting temperature. The tensile strength and modulus of cel-sal gel showed adjustable range at 0.03–0.02 MPa and 5.21–420.58 MPa, respectively. And the thermal contact resistance of the cel-sal gel displayed dynamic change, which corresponded to the dynamic variation of the modulus. Impressively, the cel-sal gel exihibited self-healing and was found to be suitable for large-scale preparation. Additionally, the cel-sal gel showed excellent performance for daily electronics (USB flash disk and CPUs) regarding thermal shock characterizations. The collected waste heat was successfully used to generate electricity and output different voltages lying within the range of 12–113 mV, showing a broad and significant impact in the field of energy materials. The selection of thermomechanical materials (Thermal energy storage materials) with suitable thermomechanical properties facilitates more efficient collection and utilization of low-grade waste heat, thereby minimizing energy waste and enhancing overall energy utilization efficiency. This work represents a new direction of Thermal energy storage materials for diverse efficient low-grade thermal management applications, and holds great potential in promoting SDGs.

Declaration of competing interest

The authors declare that they have no known competing financial interests or personal relationships that could have appeared to influence the work reported in this paper.

CRediT authorship contribution statement

Yifan Liu: Writing – review & editing, Writing – original draft, Visualization, Validation, Supervision, Software, Resources, Project administration, Methodology, Investigation, Formal analysis, Data curation, Conceptualization. **Jiazuo Zhou:** Writing – review & editing, Writing – original draft, Visualization, Validation, Supervision, Software, Resources, Project administration, Methodology, Investigation, Formal analysis, Data curation, Conceptualization. **Ziyao Wang:** Data curation. **Lei Qiao:** Data curation. **Yudong Li:** Data curation. **Yuan Yu:** Data curation. **Cong Li:** Data curation. **Jinliang Zhu:** Data curation. **Yuehe Gu:** Data curation. **Xiaohan Sun:** Data curation. **Haiyue Yang:** Funding acquisition, Data curation. **Chengyu Wang:** Funding acquisition.

Acknowledgments

This work was supported by the National Key Research and Development Program of China (No. 2023YFD2201403), the National Natural Science Foundation of China (Nos. 32171693, 32201482), China Postdoctoral Science Foundation (No. 2024T170115) and the Heilongjiang Natural Science Foundation Outstanding Youth Project (No. YQ2022C002).

Supplementary materials

Supplementary material associated with this article can be found, in the online version, at doi:10.1016/j.cclet.2025.112196.

References

[1] Y.F. Liu, J.Z. Zhou, Y.D. Li, et al., Adv. Funct. Mater. 34 (2024) 2400203.
[2] G. Wang, Z. Tang, Y. Gao, et al., Chem. Rev. 123 (2023) 6953–7024.
[3] X. Li, Y. Liu, Y. Xu, et al., Matter 6 (2023) 4050–4065.
[4] X. Hu, P. Hu, L. Liu, et al., Matter 7 (2024) 4398–4409.
[5] Z. Zeng, X. Yang, B. Zhao, et al., Energy Environ. Sci. 17 (2024) 800–812.
[6] J.J. Duan, B.Y. Yu, L. Huang, et al., Joule 5 (2021) 768–779.
[7] J. Zhou, T.G. Chen, Y. Tsurimaki, et al., Joule 7 (2023) 2830–2844.
[8] G. Martinopoulos, Sustain. Energy Technol. Assess. 69 (2024) 103921.
[9] Z. He, R. Wang, J. Wang, et al., Env. Sci. Ecotechnol. 26 (2025) 100574.
[10] C. Jiang, Z. Yan, Y. Bai, et al., NPJ Clean Water 8 (2025) 47.
[11] H. Chang, L. Tan, H. Feng, et al., Chem. Eng. J. 500 (2024) 157011.
[12] A. Li, M.K. Huang, D. Hu, et al., Chin. Chem. Lett. 34 (2023) 107916.
[13] Z. Jiang, Z. Ge, S. Yan, et al., Chin. Chem. Lett. 35 (2024) 108637.
[14] S. Gao, Y.X. Yang, A.S. Falchevskaya, et al., Adv. Sci. 11 (2024) 2306692.
[15] X. Geng, C. Wang, J. Chen, et al., ACS Nano 18 (2024) 11300–11310.
[16] Y. Liu, Z. Lv, J. Zhou, et al., Adv. Mater. 36 (2024) 2406915.
[17] Y.C. Peng, Y. Cui, Natl. Sci. Rev. 11 (2024) nwae295.
[18] Y.M. Fu, Z. Wang, K.F. Wu, et al., Chin. Chem. Lett. 36 (2025) 110479.
[19] L. Chen, X. Wei, F. Wang, et al., Chin. Chem. Lett. 33 (2022) 2635–2638.
[20] Z. Lv, X. Xia, P. Cao, et al., Chin. Chem. Lett. 37 (2026) 111282.
[21] P. Zhao, L.L. Zhu, Chin. Chem. Lett. 29 (2018) 1706–1708.
[22] B. Zhao, Z. Li, L. Zheng, et al., Chin. Chem. Lett. 35 (2024) 109810.
[23] L. Geng, J.P. Wang, X.L. Yang, et al., Chem. Eng. J. 487 (2024) 150749.
[24] Y. Zhao, Y. Chen, X. Song, et al., Adv. Funct. Mater. 33 (2023) 2214382.
[25] Y. Liu, J. Zhou, Y. Li, et al., Small 19 (2023) 2305134.
[26] J. Wei, L. Li, R. Li, et al., Int. J. Smart Nano Mater. 13 (2022) 612–625.
[27] J. Wei, R. Li, L. Li, W. Wang, T. Chen, Nano-Micro Lett. 14 (2022) 1900248.
[28] Y. Fang, Z. Bai, L. Yang, et al., Adv. Funct. Mater. 34 (2024) 2314353.
[29] J. Wang, L. Emmerich, J. Wu, P. Vana, K. Zhang, Nat. Sustain. 4 (2021) 877–883.
[30] Q. Liu, Y. Fang, X. Xiong, W. Xu, J. Cui, Angew. Chem. Int. Ed. 63 (2024) e202320095.
[31] M. Kim, S. Hong, J.J. Park, et al., Adv. Mater. 36 (2024) 2313344.
[32] Y. Fang, X. Xiong, L. Yang, et al., Adv. Funct. Mater. 33 (2023) 2301505.
[33] W. Kong, C. Wang, C. Jia, Y. Kuang, et al., Adv. Mater. 30 (2018) 1801934.
[34] H. Wang, Y. Peng, H. Peng, J.Y. Zhang, Proc. Natl. Acad. Sci. U. S. A. 119 (2022) e2200223119.
[35] G. Zhou, Y. Li, W. Chen, J. Energy Storage 74 (2023) 109381.
[36] W.F. Green, J. Phys. Chem. 12 (1908) 655–660.
[37] S. Chu, A. Majumdar, Nature 488 (2012) 294–303.
[38] Z.Y. Xu, R.Z. Wang, C. Yang, Energy 176 (2019) 1037–1043.